JPE 16-3-23

http://dx.doi.org/10.6113/JPE.2016.16.3.1056
ISSN(Print): 1598-2092 / ISSN(Online): 2093-4718

A Frequency-Tracking Method Based on a SOGI-PLL for Wireless Power Transfer Systems to Assure Operation in the Resonant State

Ping-an Tan†, Haibing He*, and Xieping Gao**

†,*School of Information Engineering, Xiangtan University, Xiangtan, China
**MOE Key Laboratory of Intelligent Computing & Information Processing, Xiangtan University, Xiangtan, China

Abstract

Wireless power transfer (WPT) technology is now recognized as an efficient means of transferring power without physical contact. However, frequency detuning will greatly reduce the transmission power and efficiency of a WPT system. To overcome the difficulties associated with the traditional frequency-tracking methods, this paper proposes a Direct Phase Control (DPC) approach, based on the Second-Order Generalized Integrator Phase-Locked Loop (SOGI-PLL), to provide accurate frequency-tracking for WPT systems. The DPC determines the phase difference between the output voltage and current of the inverter in WPT systems, and the SOGI-PLL provides the phase of the resonant current for dynamically adjusting the output voltage frequency of the inverter. Further, the stability of this control method is analyzed using the linear system theory. The performance of the proposed frequency-tracking method is investigated under various operating conditions. Simulation and experimental results convincingly demonstrate that the proposed technique will track the quasi-resonant frequency automatically, and that the ZVS operation can be achieved.

Key words: Direct Phase Control (DPC), Frequency-tracing, SOGI-PLL, Wireless Power Transfer (WPT), ZVS

I. Introduction

Wireless Power Transfer (WPT) technology is a promising technique for use in our daily lives. It gets rid of various problems, such as friction and aging. The sparks produced in power transfer are eliminated. This is advantageous since they negatively impact the lifespan of electrical equipment and pose a hazard to human safety. Furthermore, WPT can meet the requirements of some special cases, like mining and underwater operations. It also proves to be convenient in such fields as portable electronics, implanted medical instruments, sensor networks and electric vehicles [1]-[3]. However, for a typical WPT system, the inherent parameters of the resonant tank may dynamically drift away from the designed parameters due to load variations and mutual coefficient changes [4], [5]. This often results in frequency detuning. This is a problem since frequency detuning greatly reduces the transmission power and efficiency of WPT systems.

Obviously, the topics of the transmission power and efficiency are crucial for WPT systems, since they are necessary for safety and energy preservation [6], [7]. Accordingly, for the sake of large transmission power and high power-delivery efficiency, resonant frequency-tracking for WPT systems is of great significance [8]. A typical method of adaptive impedance matching is proposed in [9], which is regarded as a kind of passive tracking method. In this method, an adaptive impedance matching network based on a capacitor-matrix is introduced. This can dynamically change the impedance values to maintain a reasonable level of maximum power transfer. However, this kind of method is difficult in terms of hardware implementation. In addition, this method cannot accurately realize impedance matching.

Meanwhile, various frequency-tracking methods have been proposed in the past to assure operation in the resonant state for WPT systems. The most popular among these methods is the PLL method [10]. To track the resonant frequency, the

Manuscript received May 7, 2015; accepted Dec. 9, 2015
Recommended for publication by Associate Editor Se-Kyo Chung.
†Corresponding Author: tanpingan@xtu.edu.cn
Tel: +86-731-58292217, Xiangtan University
*School of Information Engineering, Xiangtan University, China
**MOE Key Lab. of Intelligent Computing & Information Processing, Xiangtan University, China

method of a PLL with zero-crossing detection is widely used. Unfortunately, it is sensitive to distortions and disturbances of the input signal [11], [12]. The Second-Order Generalized Integrator Phase-Locked Loop (SOGI-PLL) based on an adaptive filter is widely used in grid connected converters synchronization techniques. Compared with the traditional Phase-Locked Loop (PLL), the SOGI-PLL is less-sensitive to distortions and disturbances of the input signal [13], [14]. However, it is impossible to accurately regulate the phase difference between the output voltage and current of an inverter in WPT systems, which is not conducive to the operation of Soft-Switching. Therefore, to overcome the difficulties associated with the traditional frequency-tracking methods, this paper proposes a Direct Phase Control (DPC) approach, based on the SOGI-PLL, to provide accurate frequency-tracking for WPT systems. The DPC determines the phase difference between the output voltage and current of an inverter in WPT systems, and the SOGI-PLL provides the phase of the resonant current for dynamically adjusting the output voltage frequency of the inverter. Thus, the phase of the resonant current can be accurately detected regardless of distortions and disturbances, and the dead time imposed by the drivers can be regulated precisely. Moreover, the necessary dead time imposed by the drivers can be compatible with the resonant current phase lag control [15], [16]. With the proposed method a WPT system can track the quasi-resonant frequency automatically and the ZVS operation can be achieved.

This paper is organized in six sections. After the introduction, the resonance principle is analyzed, which mainly investigates the importance of resonance to improve transmission power and efficiency. In Section III, the frequency-tracking method is presented. The linearization and stability analysis are discussed in Section IV. In Section V, the performance of the proposed method is presented, and some conclusions and suggestions for future work are given in Section VI.

II. WPT System and Analysis

Apart from the power source and load, as shown in Fig. 1, the WPT system is mainly composed of the following three parts: the inverter, the coupler and the rectifier. Unlike traditional transformers, the primary and secondary sides of the coupler are separate from each other. The WPT system is divided into the following two parts by the coupler: the transmitting terminal and the receiving terminal. The introduction of the transmitting terminal, which consists of a DC source and a high-frequency inverter, makes it possible to provide a high-frequency AC current for the primary side of the coupler. At the receiving terminal, the rectifier and circuits of the filter are applied. With this the AC voltage that comes out of the coupler is converted into a DC voltage.

Fig. 2 shows an equivalent circuit model of the WPT system as shown in Fig. 1. According to this model, the WPT system can be expressed by the following equations.

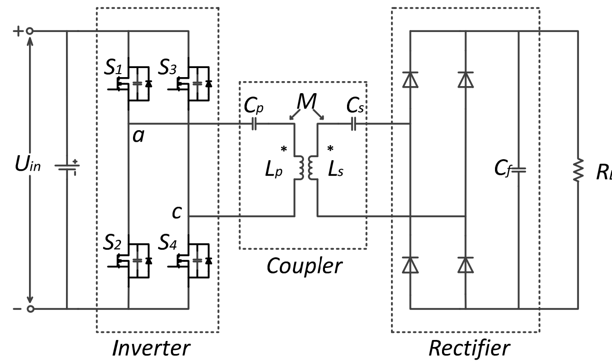

Fig. 1. Main circuit of the WPT system.

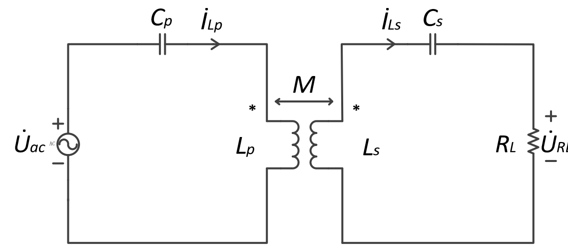

Fig. 2. Equivalent circuit model of the WPT system.

$$\dot{U}_{ac} = j\left(\omega L_p - \frac{1}{\omega C_p}\right)\dot{I}_{Lp} - j\omega M\dot{I}_{Ls} \quad (1)$$

$$j\omega M\dot{I}_{Lp} = (j\omega L_s + \frac{1}{j\omega C_s} + R_L)\dot{I}_{Ls} \quad (2)$$

Substituting (2) into (1), the input impedance of the WPT system is:

$$Z_{in} = \frac{\dot{U}_{ac}}{\dot{I}_{Lp}} = \frac{\omega^2 M^2 R_L}{\left(\omega L_s - \frac{1}{\omega C_s}\right)^2 + R_L^2} + j[\omega L_p - \frac{1}{\omega C_p} - \frac{\omega^2 M^2(\omega L_s - \frac{1}{\omega C_s})}{(\omega L_s - \frac{1}{\omega C_s})^2 + R_L^2}] \quad (3)$$

According to (3), the value of the input impedance can be expressed as:

$$|Z_{in}| = \sqrt{[\frac{\omega^2 M^2 R_L}{(\omega L_s - \frac{1}{\omega C_s})^2 + R_L^2}]^2 + [\omega L_p - \frac{1}{\omega C_p} - \frac{\omega^2 M^2(\omega L_s - \frac{1}{\omega C_s})}{(\omega L_s - \frac{1}{\omega C_s})^2 + R_L^2}]^2} \quad (4)$$

According to (3) and the principle of the inverter circuit, the RMS value of the fundamental current on the primary side can be expressed as:

$$I_{Lp} = \frac{U_{ac}}{|Z_{in}|} = \frac{2\sqrt{2}U_{in}}{\pi|Z_{in}|} \quad (5)$$

where U_{in} is the input DC voltage. Overlooking the loss of the rectifier bridge, according to (2) and (5), the output power can be expressed as:

$$P_o = I_{Ls}^2 R_L = \frac{8\omega^2 M^2 U_{in}^2 R_L}{\pi^2[\left(\omega L_s - \frac{1}{\omega C_s}\right)^2 + R_L^2]|Z_{in}|^2} \quad (6)$$

With the help of (3), the input power factor of the equivalent circuit presented in Fig.2 is:

$$\rho = \frac{P_{in}}{S_{in}} = \frac{R_{in}}{|Z_{in}|} = \frac{\omega^2 M^2 R_L}{[\left(\omega L_s - \frac{1}{\omega C_s}\right)^2 + R_L^2]|Z_{in}|} \quad (7)$$

By analyzing equations (4)-(7), the relationships between

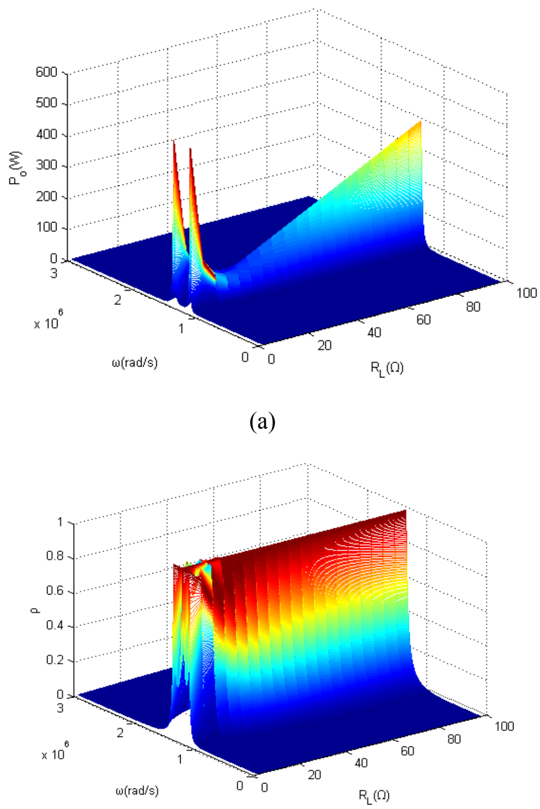

(a)

(b)

Fig. 3. (a) Output power according to R_L and ω; (b) Input power factor according to R_L and ω.

TABLE I
SPECIFICATIONS OF THE SYSTEM

Var.	Value	Description
U_{in}/V	36	input DC-link voltage
C_p/nF	10.95	transmitter-side resonant capacitor
C_s/nF	10.95	receiver-side resonant capacitor
$L_p/\mu\text{H}$	63.33	transmitter-side inductance
$L_s/\mu\text{H}$	63.33	receiver-side inductance
$M/\mu\text{H}$	12.67	mutual inductance
d/cm	10	Distance between two coils
R_L/Ω	(2,100)	load
$\omega/\text{k rad/s}$	(5,3000)	central frequency of PLL

the output power and other factors which include the frequency and load, and the relationships between the input power factor and these factors can be depicted as Fig. 3 (a)-(b) respectively. The specifications of the system are displayed in Table I.

Fig. 3 shows that the output power and the input power factor vary with respect to the factors of frequency and load. In addition, the output power obtains its maximum value at those points where the input power factor is close to one, and the WPT system works in the resonant state. Thus, for the

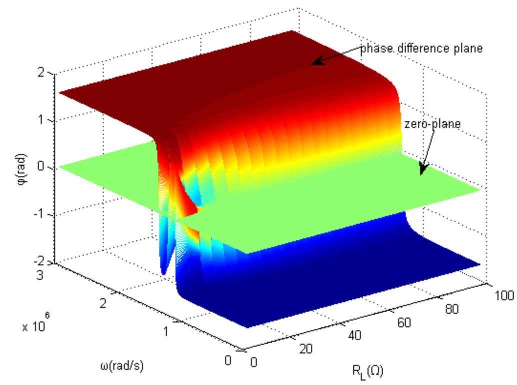

Fig. 4. Phase difference according to R_L and ω; the zero- plane.

sake of the maximum output power and high transmission efficiency, an effectively control approach should be taken to assure that the WPT system is automatically working in resonant state.

According to equation (3), the phase difference φ between the output voltage $\dot{U}_{ac}$ and current $\dot{I}_{Lp}$ of the inverter can be expressed as:

$$\varphi = tan^{-1}\left(\frac{\left(\omega L_s - \frac{1}{\omega C_s}\right)^2 + R_L^2}{\omega^2 M^2 R_L} \times \left[\omega L_p - \frac{1}{\omega C_p} - \frac{\omega^2 M^2 (\omega L_s - \frac{1}{\omega C_s})}{(\omega L_s - \frac{1}{\omega C_s})^2 + R_L^2}\right]\right) \tag{8}$$

By analyzing (8), the relationship between the phase difference and the factors, which include the frequency and load, can be depicted as in Fig. 4. When the WPT system works in the resonant state, the phase difference is zero. Accordingly, the resonant points are located in the junctions of the phase-difference plane and the zero-plane.

It is evident from (8) that the WPT system works in the resonant state when the output voltage and current of the inverter have the same phase angle. This can be realized by controlling the switching frequency of the inverter according to the resonant frequency.

III. FREQUENCY-TRACKING METHOD

In order to keep the WPT system working in the resonant state, a DPC approach, as shown in the shaded area of Fig. 5, based on the SOGI-PLL, is proposed to provide frequency-tracking. By sensing the primary side current, the output phase angle θ' of the SOGI-PLL acts as a control signal for the PWM driver. According to the cosine value of θ' the PWM driver signals V_{GS} are obtained as presented in Fig. 6. In addition, the dead angle θ_d between the two sets of gate signals $V_{GS,14}$ and $V_{GS,23}$ can be regulated precisely. Where d is a constant whose value is close to zero and the dead angle θ_d is expressed as:

$$\theta_d = 2\,sin^{-1}\,d \tag{9}$$

With the help of the proposed frequency-tracking method, the output voltage frequency of the inverter in the WPT

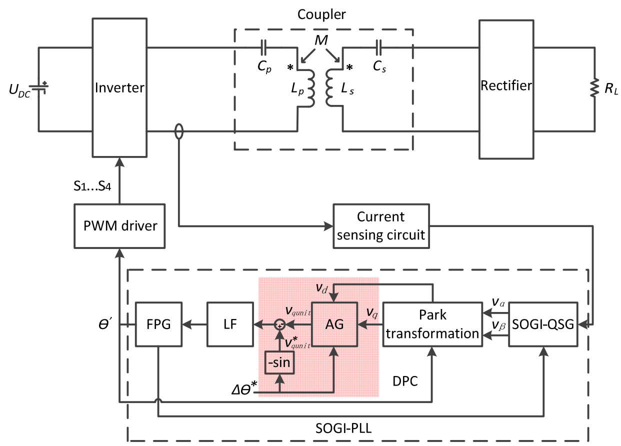

Fig. 5. Schematic diagram of frequency-tracking.

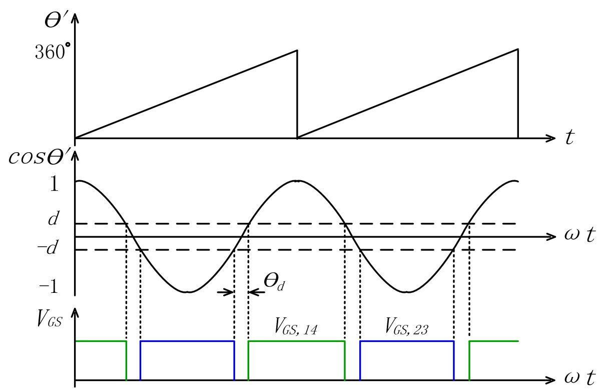

Fig. 6. Regulation of the PWM driver signals.

system can track the resonant frequency automatically if the parameter $\Delta\theta^*$ is set to zero, so that the phase difference between the output voltage and current of the inverter will be zero correspondingly. Furthermore, the phase difference can be accurately regulated by the parameter $\Delta\theta^*$.

To realize the above control strategy, the key is to obtain an accurate phase angle θ'. The proposed frequency-tracking method, as shown in Fig. 7, is composed of five parts as follows, the Second-Order Generalized Integrator Quadrature Signal Generator (SOGI-QSG), the Park transformation, the DPC, the Low-pass Filter (LF), and the Frequency/Phase-Angle Generator (FPG). The proposed method has two feedback loops, where the FPG provides the phase and central frequency for the Park transformation and the SOGI-QSG, respectively [17], [18]. The introduction of the SOGI-QSG improves the phase detection performance.

A. SOGI-QSG

The SOGI-QSG is a kind of Adaptive Filter (AF). A traditional filter can only deal with signals that lie in the fixed frequency range. What is worse, the parameters of this kind of filter are static and their values are assigned during the design progress of the filter. However, an AF can adapt its parameters automatically according to the optimization algorithm. In addition, during the design process of an AF, information on the signal to be filtered is not needed [19], [20]. The SOGI-QSG can deal with signals that lie in any frequency range. Moreover, it can be used in occasions with distortions and disturbances.

According to Fig. 7, the transfer functions of the SOGI-QSG can be expressed as:

$$D(s) = \frac{v'}{v}(s) = \frac{k\omega' s}{s^2 + k\omega' s + \omega'^2} \tag{10}$$

$$Q(s) = \frac{qv'}{v}(s) = \frac{k\omega'^2}{s^2 + k\omega' s + \omega'^2} \tag{11}$$

where ω' represents the central frequency of the SOGI and k is the gain of the SOGI-QSG.

Suppose that the input signal with distortion is:

$$v = \sum_{n=1}^{m} v_n = \sum_{n=1}^{m} V_n \cos(n\omega t + \emptyset_n) \tag{12}$$

where V_n, $n\omega$, and $\emptyset_n$ represents the amplitude, angular frequency and initial phase angle of the nth harmonic v_n of the input signal v, respectively. As a result, the nth harmonic can be indicated as a phasor $\dot{v}_n$, and the amplitude, angular frequency and initial phase angle are V_n, $n\omega$ and $\emptyset_n$, respectively. With the help of (10) and (11), the outputs of the SOGI-QSG can be expressed as:

$$\dot{v}_n' = \dot{D}\dot{v}_n, \begin{cases} |\dot{v}_n'| = \dfrac{kn\omega'\omega V_n}{\sqrt{(kn\omega'\omega)^2 + ((n\omega)^2 - \omega'^2)^2}} \\ \angle\dot{v}_n' = tan^{-1}\left(\dfrac{\omega'^2 - (n\omega)^2}{kn\omega'\omega}\right) + \emptyset_n \end{cases} \tag{13a}$$

$$q\dot{v}_n' = \dot{Q}\dot{v}_n, \begin{cases} |q\dot{v}_n'| = \dfrac{\omega'}{n\omega}|\dot{v}_n'| \\ \angle q\dot{v}_n' = \angle\dot{v}_n' - \dfrac{\pi}{2} \end{cases} \tag{13b}$$

Once the value of the angular frequency ω is equal to the central frequency ω', equation (13) can be calculated as:

$$\dot{v}_n' = \dot{D}\dot{v}_n, \begin{cases} |\dot{v}_n'| = \dfrac{kV_n}{\sqrt{(k^2-2) + n^2 + \frac{1}{n^2}}} \\ \angle\dot{v}_n' = \tan^{-1}(\dfrac{1-n^2}{kn}) + \emptyset_n \end{cases} \tag{14a}$$

$$q\dot{v}_n' = \dot{Q}\dot{v}_n, \begin{cases} |q\dot{v}_n'| = \dfrac{1}{n}|\dot{v}_n'| \\ \angle q\dot{v}_n' = \angle\dot{v}_n' - \dfrac{\pi}{2} \end{cases} \tag{14b}$$

For a critically-damped response $k = \sqrt{2}$ is chosen as shown in the bode diagram presented in Fig. 8. This value presents a valuable selection in terms of the setting time and overshoot limitation [17], [18]. It can be observed that the SOGI-QSG possesses the band-pass filtering property. The bandwidth of the SOGI-QSG relies on the gain k rather than the central frequency ω'. As a result, it is suitable for occasions with frequency variations.

From (14), it can be observed that the input signal has the same angular frequency as the central frequency at $n = 1$, and that the amplitudes of the outputs share the same values with the input signal. Otherwise, the amplitudes will decay obviously at $n \neq 1$. In addition, there is a phase difference of $\pi/2$ between the signals v_n' and qv_n'. Furthermore, the two orthogonal signals have the same amplitudes as v_n, while the

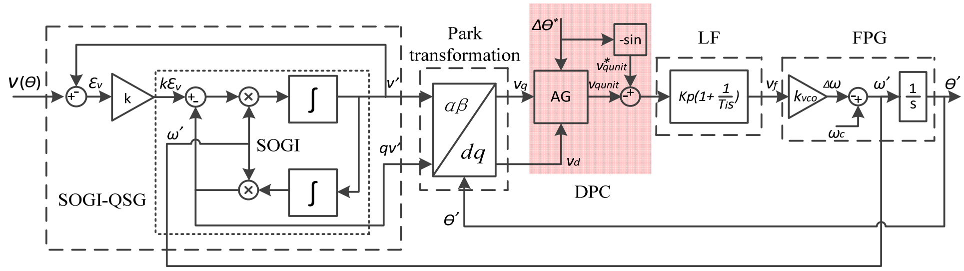

Fig. 7. Proposed frequency-tracking method.

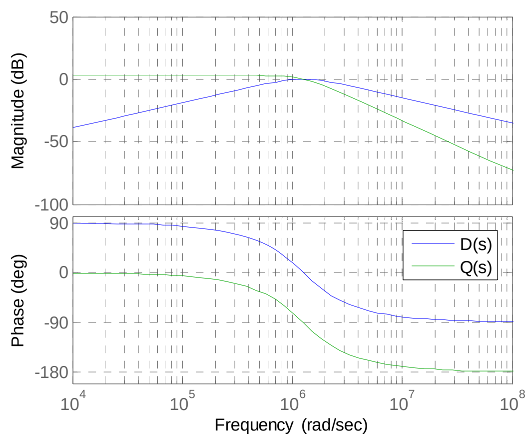

Fig. 8. Bode plot of SOGI-QSG ($k = \sqrt{2}$, $\omega' = 400000\pi$).

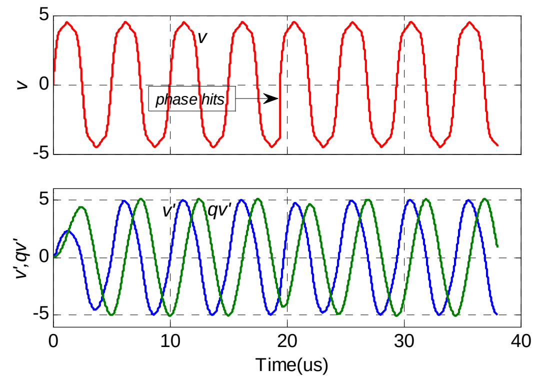

Fig. 9. Waveforms of the input signal v and the two outputs v' and qv' of SOGI-QSG, where $v = 5\cos(\omega t - \pi/2) + 0.8\cos(3\omega t - \pi/2) + 0.3\cos(5\omega t - \pi/2)$, $\omega = \omega' = 400000\pi\ rad/s$ and $k = \sqrt{2}$.

input frequency is equal to the central frequency ω'. Thus, the outputs of the SOGI-QSG can be expressed as:

$$\begin{bmatrix} v' \\ qv' \end{bmatrix} = V\begin{bmatrix} \cos\theta \\ \sin\theta \end{bmatrix} = V_1\begin{bmatrix} \cos(\omega t + \emptyset_1) \\ \sin(\omega t + \emptyset_1) \end{bmatrix} \quad (15)$$

where V and θ are the amplitude and phase of the input signal, respectively. They are equal to the values of the fundamental component of the input signal, whose amplitude, angular frequency and initial phase angle are V_1 , ω and $\emptyset_1$, respectively.

The dynamic response of the SOGI-QSG is presented in Fig. 9, where $v = 5\cos(\omega t - \pi/2) + 0.8\cos(3\omega t - \pi/2) + 0.3\cos(5\omega t - \pi/2)$, and a disturbance of $\pi/4$ leading phase hits is applied at 19.4 µs. It is evident that the SOGI-QSG can work well regardless of distortions and disturbances.

B. Park Transformation

Fig. 10 shows the Park transformation schematic diagram. There are two coordinates, including the stationary coordinates and the rotating coordinates, where θ represents the phase angle of the input signal and θ' is the output phase angle of the SOGI-PLL.

$$\begin{bmatrix} v_\alpha \\ v_\beta \end{bmatrix} = \begin{bmatrix} v' \\ qv' \end{bmatrix} \quad (16)$$

According to the Park transformation principle, the dq components are obtained by:

$$\begin{bmatrix} v_d \\ v_q \end{bmatrix} = \begin{bmatrix} \cos\theta' & \sin\theta' \\ -\sin\theta' & \cos\theta' \end{bmatrix}\begin{bmatrix} v_\alpha \\ v_\beta \end{bmatrix} \quad (17)$$

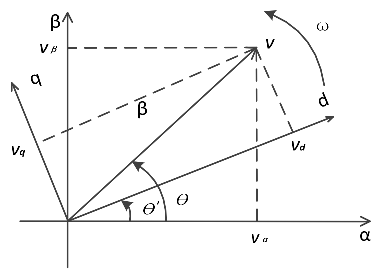

Fig. 10. The schematic diagram of Park transformation.

Substitute (15), (16) into (17) and the dq components are:

$$\begin{bmatrix} v_d \\ v_q \end{bmatrix} = V\begin{bmatrix} \cos(\theta' - \theta) \\ -\sin(\theta' - \theta) \end{bmatrix} \quad (18)$$

By analyzing (18), the value of v_q reveals the difference between the output phase θ' and the input phase θ of the PLL. According to Fig. 10 it can be seen that:

(1)At the moment when $v_q < 0$, the axis d is ahead of v, and the frequency of the PLL should be reduced.

(2)At the moment when $v_q > 0$, the axis d lags behind v, and the frequency of the PLL should be increased.

(3)At the moment when $v_q = 0$, the axis d is collinear with v.

C. DPC

For the high-frequency applications in WPT systems, in order to decrease the switching losses, it is essential to assure operation in the Soft-Switching mode. In addition, a dead

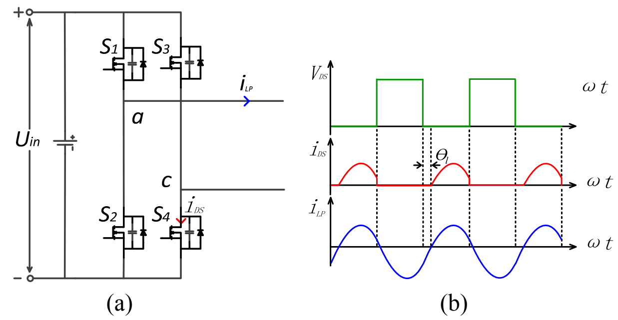

Fig. 11. (a) Inverter of WPT system, (b) ZVS operation.

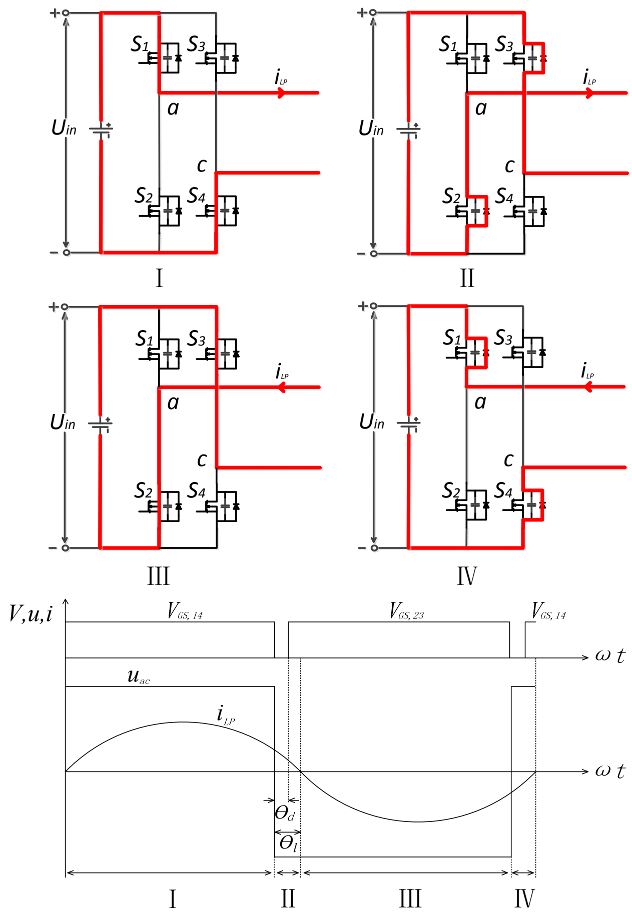

Fig. 12. ZVS operation sequence.

time in the voltage source bridge inverter is required to prevent shoot-through current [15], [16]. The inverter of WPT system is presented in Fig. 11(a), and the ZVS operation is introduced as shown in Fig. 11(b).

Fig. 11(b) shows that a resonant current phase lag θ_l is introduced where V_{DS} and i_{DS} represent the voltage across the MOSFET and the current through the MOSFET, respectively, and i_{LP} repesents the output resonant current of the inverter. The phase lag θ_l refers to the difference between the zero-crossing point of the current i_{DS} and the falling edge of the voltage V_{DS}. The voltage across the MOSFET is zero if the MOSFET turn on during the phase lag θ_l, and then the ZVS operation is achieved.

In a real circuit, the phase lag θ_l is redefined as the difference between the zero-crossing point of the output resonant current i_{LP} and the falling edge of the driver signal of the MOSFET as shown in Fig. 12. In order to assure the ZVS operation, it is very important that the phase lag θ_l should be greater than the dead angle θ_d.

In this paper, the Adaptive Gain (AG) is used and it can be expressed as:

$$AG = \begin{cases} \frac{cos(\Delta\theta^*)}{v_d} & , v_d \neq 0 \\ 1 & , v_d = 0 \end{cases} \tag{19}$$

where $\Delta\theta^*$ is the reference value of the phase difference between the output and input signal of the SOGI-PLL, and v_d is one of the dq components of the Park transformation.

In addition, the component of v_{qunit}, as shown in Fig.7, can be expressed as:

$$v_{qunit} = v_q AG \tag{20}$$

According to (18)-(20), the actual phase difference $\Delta\theta$ is:

$$\Delta\theta = \theta' - \theta = tan^{-1}[-\frac{v_{qunit}}{cos(\Delta\theta^*)}] \tag{21}$$

At the moment when the SOGI-PLL operates steadily, as shown in Fig. 7, the condition of $v_{qunit} = -sin(\Delta\theta^*)$ is satisfied. With equation (21), $\Delta\theta = \Delta\theta^*$. Thus, it is possible to regulate the actual phase difference $\Delta\theta$ by setting the parameter $\Delta\theta^*$, as presented in Fig. 13.

The DPC makes it possible for the resonant current phase lag angle θ_l to have the same value as the parameter $\Delta\theta^*$. Once the dead angle has been assigned, the parameter of $\Delta\theta^*$ should be set so that it is greater than θ_d. On the other hand, for the sake of resonant frequency-tracking, the minimum input power factor ρ_{min}, which is close to one, is introduced. Therefore, the parameter of $\Delta\theta^*$ should be given by:

$$2\,sin^{-1} d < \Delta\theta^* < \cos^{-1}(\rho_{min}) \tag{22}$$

Thus, the dead time imposed by the drivers is compatible with that of the resonant current phase lag control. In this case, the WPT system operates in a quasi-resonant state and the ZVS operation is achieved.

IV. Linearization and Stability Analysis

According to Fig. 13, some relationships can be depicted as the following equations.

$$\varepsilon = -v_{qunit} = -sin(\theta - \theta') \tag{23}$$

Once the component v_{qunit}, as shown in (23), is small enough the equation can be depicted as:

$$\varepsilon = -(\theta - \theta') \tag{24}$$

As for the FPG component, which works as the voltage controlled oscillator (VCO) of a PLL, the output frequency is:

$$\omega' = \omega_c - \Delta\omega = \omega_c - k_{vco} v_f \tag{25}$$

where ω_c is the central frequency of the VCO and its value relies on the frequency range of the signal to be detected. $\Delta\omega$ represents the frequency compensation, which achievs robust operation for frequency variations. k_{vco} is

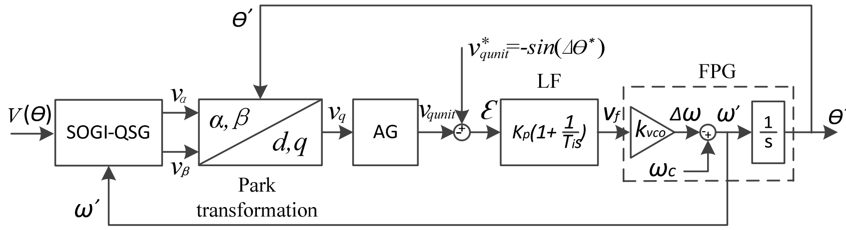

Fig. 13. Block diagram of the proposed method.

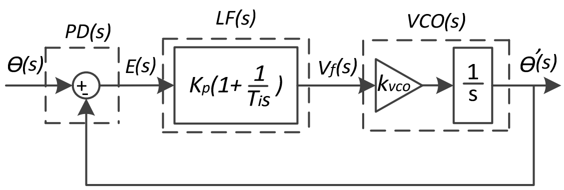

Fig. 14. Linear PLL loop.

the gain of the VCO and it works as an input sensitivity parameter. The parameter scales the input voltage. Thus, it controls the shift from the central frequency. The unit of the parameter is in radians per volt.

Therefore, a small fluctuation of the output frequency is:

$$\tilde{\omega}' = -k_{vco}\tilde{v}_f \tag{26}$$

Thus, a small fluctuation of the phase angle is:

$$\tilde{\theta}'(t) = \int \tilde{\omega}' dt = -\int k_{vco}\tilde{v}_f dt \tag{27}$$

With the introduction of the Laplace Transform, equations (24) and (27) can be respectively converted as:

$$E(s) = -(\theta(s) - \theta'(s)) \tag{28}$$

$$\theta'(s) = -k_{vco}V_f(s)\frac{1}{s} \tag{29}$$

In addition, another relationship in terms of the component of the LF can be expressed as:

$$V_f(s) = k_p\left(1 + \frac{1}{T_i s}\right)E(s) \tag{30}$$

Accordingly, the linearization for the SOGI-PLL, as shown in Fig.13, can be presented in Fig. 14. In Fig. 14 the combination of the SOGI-QSG, the Park transformation and the AG works as a special Phase Detector (PD). A PI controller works as a Low-pass Filter. The Frequency/Phase-Angle Generator (FPG) works as the voltage controlled oscillator (VCO).

The closed-loop transfer function of the linearized PLL can be expressed as:

$$G(s) = \frac{Ks + \frac{K}{T_i}}{s^2 + Ks + \frac{K}{T_i}} \tag{31}$$

$$K = k_p k_{vco} \tag{32}$$

where k_p is the proportional gain and T_i is the integral time constant of the PI controller.

The natural frequency and the damping ratio are:

$$\omega_n = \sqrt{\frac{K}{T_i}} \tag{33}$$

$$\xi = \frac{\sqrt{KT_i}}{2} \tag{34}$$

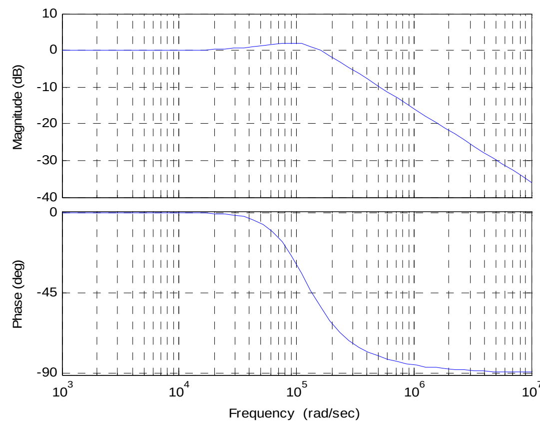

Fig. 15. Bode plot of the PLL system.

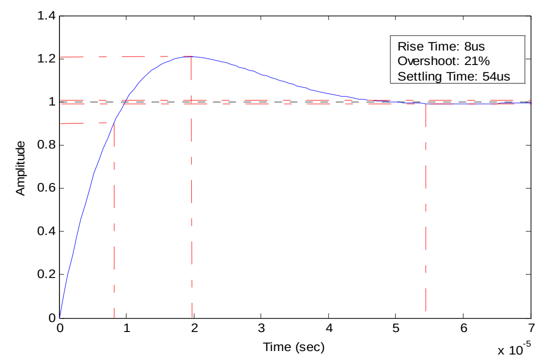

Fig. 16. Step response of the PLL system.

For a good transient response, a damping ratio $\xi = 0.7$ is advisable. Allow for the lock range of the PLL as depicted in (35). The natural frequency ω_n should not be too low.

$$\Delta\omega_L \approx 2\xi\omega_n \tag{35}$$

In addition, the lock time, as presented in (36), is another issue that needs to be taken into account.

$$T_L \approx \frac{2\pi}{\omega_n} \tag{36}$$

According to the criteria in the previous analysis, a natural frequency of $\omega_n = 113140 rad/s$ is chosen. According to (35), (36) $\Delta\omega_L \approx 160000 rad/s$, $T_L \approx 54us$, the bode plot and the step response are displayed in Fig. 15 and Fig. 16, respectively.

With the help of Fig. 15 it is possible to obtain some information about the PLL system. Firstly, the low-frequency

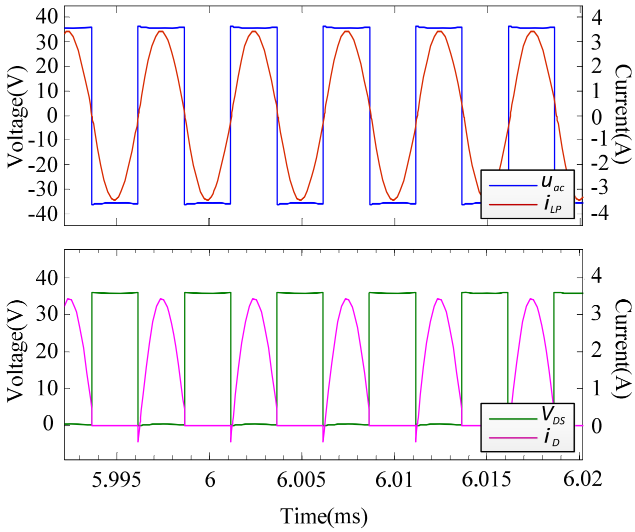

Fig. 17. Waveforms of u_{ac} and i_{Lp}; Waveforms of the voltage and current of MOSFET operates in ZVS mode.

gain of the closed-loop PLL is nearly 0. As a result, when it works under steady working conditions, the PLL system is extremely accurate. Secondly, it has a peak value of 2.3dB at the resonant point. This indicates that the PLL system shows a low overshoot. Thirdly, because of its wide bandwidth a good transient response is obtained. In addition, the system has a large lock range indicating that the PLL can get locked in a single beat with a high initial frequency deviation. As shown in Fig. 16, the system shows a good transient response and a low overshoot.

V. Performances and Results Analysis

A. *Simulation Results Analysis*

In order to verify the proposed method discussed above, simulations have been done according to Fig. 5. The main parameters for the simulated system are presented in Table I. In this experiment the load is $R_L = 16\Omega$ and the central frequency of PLL is $f_c = 200\text{kHz}$.

The WPT system, which operates with the DPC approach, works in a quasi-resonant state after setting the parameters as discussed above. As a result, the current out of the inverter is approximately in phase with the voltage as shown in Fig. 17. The waveforms of the voltage and current of the MOSFET are displayed at the bottom of Fig. 17. It is obvious that the ZVS operation for the inverter of the WPT system is achieved.

The load R_L changes from 16 Ω to 8 Ω at 6ms. Fig. 18(a) provides the waveforms of the WPT system without the DPC. As shown in Fig. 18(a), the transmitter-side voltage u_{ac} is not synchronized with the transmitter-side current i_{Lp} when the load R_L changes. Fig. 18(b), (c), and (d) display some simulation performances of the WPT system operating with the DPC. Fig. 18(b) and (c) show that the phase difference between the voltage u_{ac} and the current i_{Lp} of the

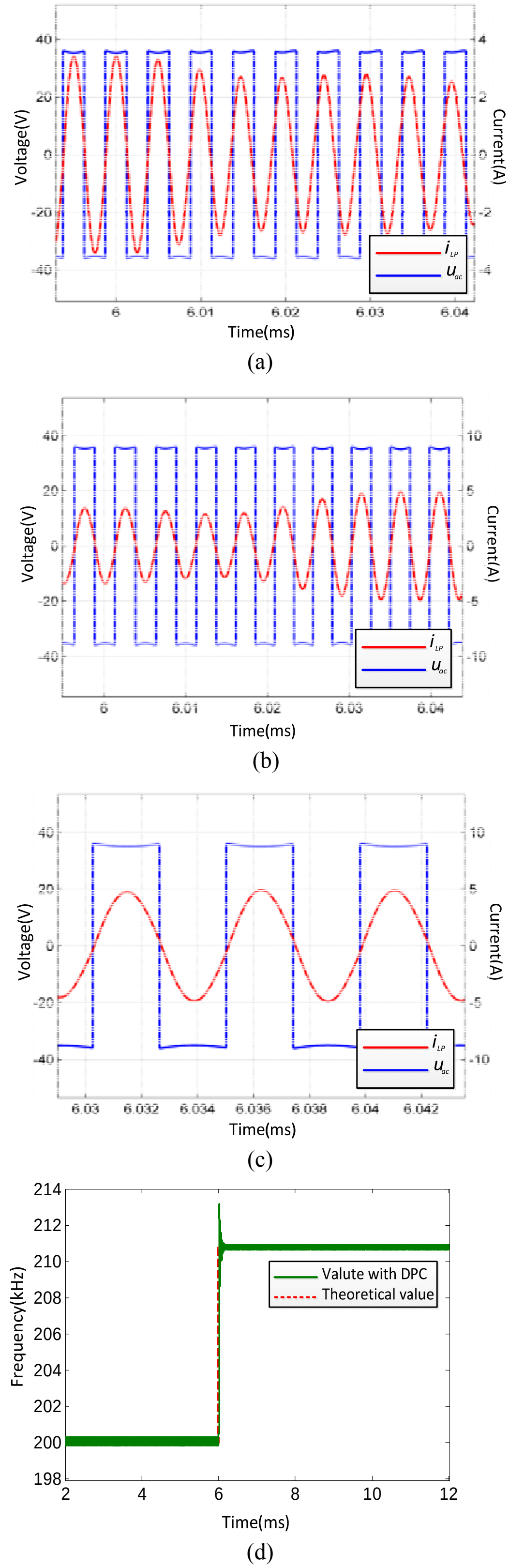

Fig. 18. Waveforms when R_L changes from 16Ω to 8Ω(a) Waveforms of u_{ac} and i_{Lp} (without DPC); (b) Waveforms of u_{ac} and i_{Lp} (with DPC); (c) Magnification of one segment of waveforms of u_{ac} and i_{Lp} (with DPC); (d) Frequency variations behavior.

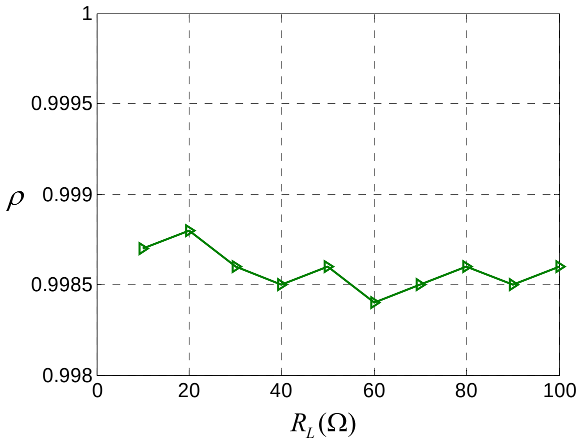

Fig. 19. The input power factor ρ according to R_L.

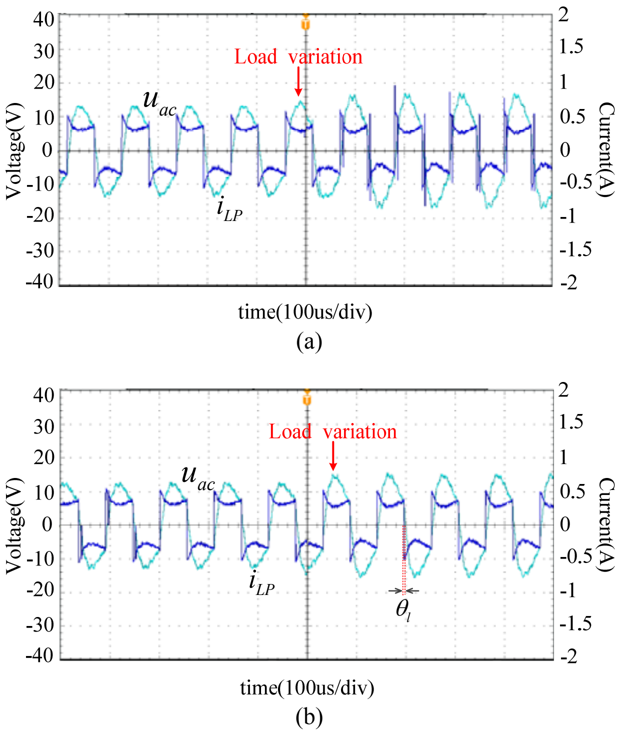

Fig. 20. Waveforms of u_{ac} and i_{Lp} when R_L changes from 16Ω to 8Ω (a) without DPC; (b) with DPC.

transmitter-side returns approximately to zero at the end of the transition during which the load R_L changes from 16 Ω to 8 Ω. Fig. 18(d) shows that at the end of the transition, the frequency can be tracked automatically.

Changes in the load R_L and its effect on the input power factor ρ expressed in (6) are displayed in Fig. 19.

Fig. 19 shows that the factor ρ is approximately equal to one and stabilized enough. This indicates that the WPT system works in a quasi-resonant state steadily with a stable phase difference between the output voltage and current of the inverter. This is essential for the implementation of the ZVS operation.

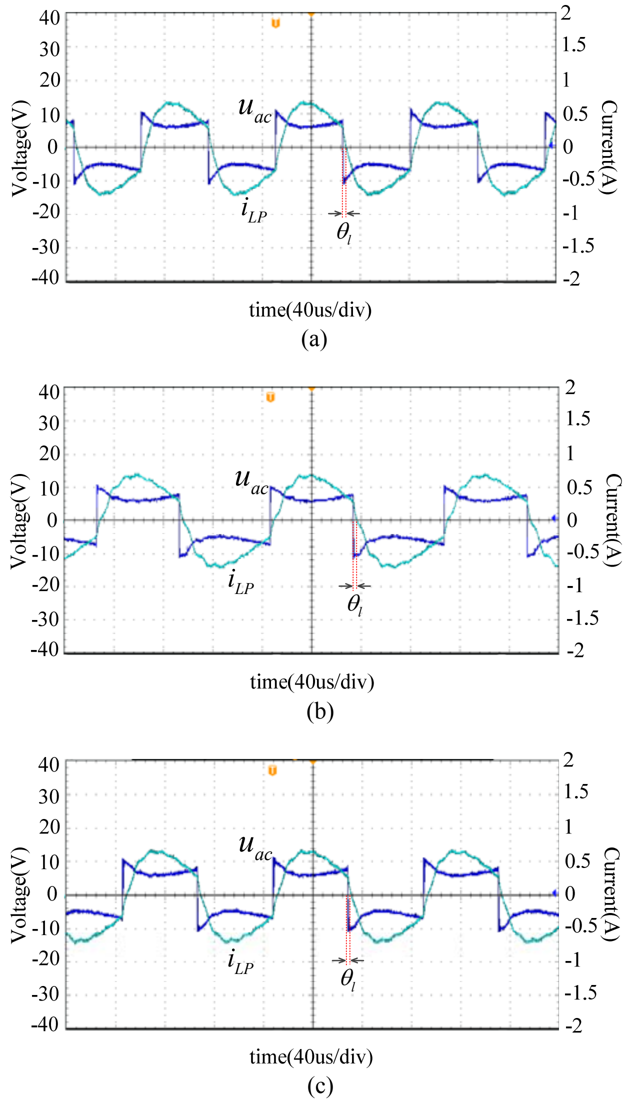

Fig. 21. Waveforms of u_{ac} and i_{Lp} with DPC (a) waveforms without any parameter variations; (b) waveforms with distance variation between primary-side and secondary-side; (c) waveforms with misalignment between primary-side and secondary-side.

B. *Experimental Results Analysis*

In order to further verify the validity of the proposed technique, a hardware implementation has been done and the obtained experimental results are presented in this paper. The load R_L changes from 16 Ω to 8 Ω. Fig. 20(a) shows waveforms of the frequency-tracking system without the DPC. As shown in Fig. 20(a), the transmitter-side voltage u_{ac} is not synchronized with the transmitter-side current i_{Lp} at the moment when the load R_L changes. What is worse, when the voltage swings back and forth, the ZVS operation is doomed to fail. Fig. 20(b) displays the waveforms of the system operating with the DPC. Fig. 20(b) shows that the phase difference between the voltage u_{ac} and the current i_{Lp} remains approximately zero when the load R_L changes.

In addition, a stable and slight phase lag-angle θ_l is introduced, which results in successful ZVS operation. It is obvious that the system can track the frequency automatically at the moment when the load changes.

Fig. 21(a) shows waveforms of the proposed frequency-tracking system without any parameter changes. By analyzing these waveforms it can be seen that the system can track the frequency automatically, and that the ZVS operation can be achieved simultaneously.

In addition, the performance of the proposed algorithm under both distance variations and source-target misalignment has been presented.

The distance between the two coils changes from 10cm to 5cm and the waveforms are presented in Fig. 21(b). Fig. 21(b) shows that the phase difference between the voltage u_{ac} and the current i_{Lp} remains approximately zero when the distance between the two coils changes. In addition, a stable and slight phase lag-angle θ_l is introduced, which results in successful ZVS operation.

Secondly, the receiving coil deviated from the central axis of the two coils by about 5cm and the waveforms are presented in Fig. 21(c). Similarly, Fig. 21(c) shows that the phase difference between the voltage u_{ac} and the current i_{Lp} remains approximately zero when the receiving coil deviated from its best position. In addition, a stable and slight phase lag-angle θ_l is introduced, resulting in successful ZVS operation.

It is obvious that with the proposed method, the system can track the frequency automatically when the distance between the two coils changes and when the receiving coil deviates from its best position. The ZVS operation can be achieved simultaneously.

VI. Conclusions and Future Works

In this paper, the importance of resonant frequency-tracking to a WPT system has been discussed and a DPC approach, based on the SOGI-PLL, to provide accurate frequency-tracking for WPT systems is proposed. The DPC determines the phase difference between the output voltage and current of the inverter in a WPT system, and the SOGI-PLL provides the phase of the resonant current for dynamically adjusting the output voltage frequency of the inverter. The phase of the resonant current can be detected accurately regardless of distortions or disturbances. The phase difference of a WPT system and the dead angle imposed by the drivers can be regulated precisely. Moreover, the necessary dead time imposed by the drivers is compatible with the resonant current phase lag control. With the proposed method a WPT system can track the quasi-resonant frequency automatically and the ZVS operation can be achieved. This method can be used on occasions when the load has changed and when the resonant parameters have changed. With the proposed frequency-tracking method the maximum transmission power and power-delivery efficiency of a WPT system can be obtained. This is of significance for the research and application of WPT systems.

The validity of the proposed technique has been demonstrated with simulation and experimental results. However, there is still something to do to improve the performances during the experimental process. Firstly, the switching frequency can be promoted if a much more efficient processor, such as a FPGA, is applied. Secondly, with the proposed DPC method, phase compensation can be achieved exactly and it will need to be exploited in the future. It is significant to deal with the phase delay derived from the hardware implementation. In the future, the switching frequency of the inverter will be improved in the frequency-tracking system and the phase compensation will be implemented.

The proposed method has many advantages for the WPT applications. However, there are still some possible limitations in the proposed method. Firstly, the SOGI-PLL is a computationally expensive and time-consuming algorithm. In order to apply it to WPT applications whose operating frequency is high, a much more efficient processor has to be applied which will increase the cost of the WPT system. Secondly, protective measures have to be taken to prevent damage to the processor and other control circuit during the hardware implementation. Thirdly, the proposed method can be applied on occasions when the output current is sinusoidal.

Acknowledgment

This work was supported by National Natural Science Foundation of China (NSFC) (51207134). The authors would like to thank the associate editor and the peer reviewers for their constructive suggestions which significantly improve the quality of this paper.

References

[1] A. Kurs, A. Karalis, R. Moffatt, J. D. Joannopoulos, P. Fisher, and M. Soljacic, "Wireless power transfer via strongly coupled magnetic resonances," *Science*, Vol. 317, No. 5834, pp. 83-86, Jul. 2007.

[2] J. Shin, S. Shin, Y. Kim, S. Ahn, S. Lee, G. Jung, S.-J. Jeon, and D.-H. Cho, "Design and implementation of shaped magnetic-resonance-based wireless power transfer system for roadway-powered moving electric vehicles," *IEEE Trans. Ind. Electron.*, Vol. 61, No. 3, pp.1179-1192, Mar. 2014.

[3] Y. Zhang and Z. Zhao, "Frequency splitting analysis of two-coil resonant wireless power transfer," *IEEE Antennas Wireless Propag. Lett.*, Vol. 13, pp.400-402, Mar. 2014.

[4] J. U. W. Hsu, A. P. Hu, and A. Swain, "Fuzzy logic-based directional fullrange tuning control of wireless power pickups," *IET Power Electron.*, Vol. 5, No. 6, pp. 773–781, Jul. 2012.

[5] X. Dai and Y. Sun, "An accurate frequency tracking method based on short current detection for inductive power transfer system," *IEEE Transa. Ind. Electron*., Vol. 61, No. 2, pp. 776-783, Feb. 2014.
[6] M. Solja, E. H. Rafif, and A. Karalis, "Coupled-mode theory for general free-space resonant scattering of waves," *Physical Review*, Vol. 75, No. 5, pp. 1-5, May 2007.
[7] A. Karalis, J. D. Joannopoulos, and M. Soljai, "Efficient wireless non-radiative mid-range energy transfer," *Annals of Physics*, Vol. 323, No. 1, pp. 34-48, Jan. 2008.
[8] B. Klaus, B. Lang, and T. Leibfried, "Technical analysis of frequency tracking possibilities for contactless electric vehicle charging," in *IEEE Innovative Smart Grid Technologies – Asia(ISGT ASIA)*, pp. 577-582, 2014.
[9] Y. Lim, H. Tang, S. Lim, and J. Park, "An adaptive impedance-matching network based on a novel capacitor matrix for wireless power transfer," *IEEE Trans. Power Electron*., Vol. 29, No. 8, pp. 4403-4413, Aug. 2014.
[10] R. Bosshard, J. W. Kolar, and B. Wunsch, "Control method for inductive power transfer with high partial-load efficiency and resonance tracking," in *International Power Electronics Conference (IPEC-Hiroshima)*, pp. 2167-2174, May 2014.
[11] J.-W. Yuan and Z.-Y. Lu, "Research on a novel single phase PLL strategy," *Power Electronics*, Vol. 45, No. 7, pp. 81-83, Jul. 2011.
[12] L. N. Arruda, S. M. Silva, and B. J. C. Filho, "PLL structures for utility connected systems," in *IEEE Industry Applications Conference,* Vol. 4, pp. 2655-2660, Sep./Oct. 2001.
[13] S. A. O. d. Silva. L. B. C. Campanhol, A. Goedtel, C. F. Nascimento, and D. Paiao, "A comparative analysis of p-PLL algorithms for single-phase utility connected systems," in *13th European Conference on Power Electronics and Applications(EPE)*, pp. 1-10, 2009.
[14] A. Gupta, A. Porippireddi, V. U. Srinivasa, A. Sharma, and M. Kadam, "Comparative study of single phase PLL algorithms for grid synchronization applications," *International Journal of Electronics & Communication Technology (IJECT)*, Vol. 3, No. 4, pp. 237-245, Oct./ Nov./Dec. 2012.
[15] V. M. Lopez, A. Navarro-Crespin, R. Schnell, C. Branas, F. J. Azcondo, and R. Zane, "Current phase surveillance in resonant converters for electric discharge applications to assure operation in zero-voltage-switching mode," *IEEE Trans. Power Electron.*, Vol. 27, No. 6, pp. 2925-2935, Jun. 2012.
[16] Y. Yin and R. Zane, "Digital phase control for resonant inverters," *IEEE Power Electron. Lett.*, Vol. 2, No. 2, pp. 51-53, Jun. 2004.
[17] P. Rodriguez, R. Teodorescu, I. Candela, A. V. Timbus, M. Liserre, and F. Blaabjerg, "New positive-sequence voltage detector for grid synchronization of power converters under faulty grid conditions," in *37th IEEE Power Electronics Specialists Conference (PESC)*, pp. 1-7, 2006.
[18] M. Ciobotaru, R. Teodorescu, and F. Blaabjerg, "A new single-phase PLL structure based on second order generalized integrator," in *37th IEEE Power Electronics Specialists Conference(PESC)*, pp. 1-6, 2006.
[19] A. M. Salamah, S. J. Finney, and B. W. Williams, "Three-phase phase-lock loop for distorted utilties," *IET Electric Power Appl.*, Vol. 1, No. 6, pp. 937-945, Nov. 2007.
[20] S. S. Haykin, *Aaptive Filter Theory*, Upper Saddle River, NJ: Prentice Hall, 2002.

Ping-an Tan received his B.S. and M.S. degrees in Electrical Engineering from Xiangtan University, Xiangtan, China, in 2001 and 2004, respectively; and his Ph.D. degree in Electrical Engineering from the South China University of Technology, Guangzhou, China, in 2010. Since 2011, he has been an Associate Professor in the School of Information Engineering, Xiangtan University. His current research interests include wireless power transfer, power electronics, and nonlinear control.

Haibing He was born in China, in 1989. He received his B.S. degree in Automation from Xiangtan University, Xiangtan, China, in 2013; where he is expected to receive his M.S. degree in Electrical Engineering, in 2016. His current research interests include wireless power transfer, DC-DC converters and switched-mode power supplies.

Xieping Gao was born in 1965. He received his B.S. and M.S. degrees from Xiangtan University, Xiangtan, China, in 1985 and 1988, respectively; and his Ph.D. degree from Hunan University, Changsha, China, in 2003. He is presently working as a Professor in the College of Information Engineering, Xiangtan University. He was a Visiting Scholar at the National Key Laboratory of Intelligent Technology and Systems, Tsinghua University, Beijing, China, from 1995 to 1996; and in the School of Electrical and Electronic Engineering, Nanyang Technological University, Singapore, from 2002 to 2003. He is a regular reviewer for several journals and he has been a member of the technical committees of several scientific conferences. He has authored or co-authored over 80 journal papers, conference papers, and book chapters. His current research interests include wavelet analysis, neural networks, evolution computation, and image processing.